

# Carbon use efficiencies and allocation strategies in *Prochlorococcus marinus* strain PCC 9511 during nitrogen-limited growth

Kristina Felcmanová<sup>1,2</sup>  · Martin Lukeš<sup>1,2</sup> · Eva Kotabová<sup>1</sup> · Evelyn Lawrenz<sup>1</sup> · Kimberly H. Halsey<sup>3</sup> · Ondřej Prášil<sup>1,2</sup> 

Received: 15 March 2017 / Accepted: 1 July 2017 / Published online: 18 July 2017  
© Springer Science+Business Media B.V. 2017

**Abstract** We studied cell properties including carbon allocation dynamics in the globally abundant and important cyanobacterium *Prochlorococcus marinus* strain PCC 9511 grown at three different growth rates in nitrogen-limited continuous cultures. With increasing nitrogen limitation, cellular divinyl chlorophyll *a* and the functional absorption cross section of Photosystem II decreased, although maximal photosynthetic efficiency of PSII remained unaltered across all N-limited growth rates. Chl-specific gross and net carbon primary production were also invariant with nutrient-limited growth rate, but only 20% of Chl-specific gross carbon primary production was retained in the biomass across all growth rates. In nitrogen-replete cells, 60% of the assimilated carbon was incorporated into the protein pool while only 30% was incorporated into carbohydrates. As N limitation increased, new carbon became evenly distributed between these two pools. While many of these physiological traits are similar to those measured in other algae, there are also distinct differences, particularly the lower overall efficiency of carbon utilization. The latter provides new information needed for understanding and

estimating primary production, particularly in the nutrient-limited tropical oceans where *P. marinus* dominates phytoplankton community composition.

**Keywords** *Prochlorococcus marinus* · Cyanobacteria · Primary production · Nitrogen limitation · Carbon allocation

## Introduction

Phytoplankton biomass in the oceans represents approximately 0.2% of the global photosynthetically active carbon biomass (Field et al. 1998). Despite this fact, oceans contribute 45–50% of global net primary production (NPP), equating to roughly 50 petagrams of carbon per year (Falkowski et al. 1998; Field et al. 1998). Accurate measurements of phytoplankton primary production are critical to understand and predict how marine ecosystems will respond to climate change. Furthermore, advancing ocean biogeochemistry and ecosystem models require quantitative descriptions of phytoplankton properties during resource-limited growth (Litchman and Klausmeier 2008; Follows and Dutkiewicz 2011).

*Prochlorococcus marinus* is a globally important and extensively studied cyanobacterium (Hess et al. 2001; Ting et al. 2002; Partensky and Garczarek 2010). With an average cell diameter of 0.6 μm, it is the smallest known unicellular phototroph (Chisholm et al. 1988), and is ubiquitously distributed in the euphotic zone in tropical and subtropical oligotrophic waters between 40°N and 40°S with cell densities ranging from 10<sup>4</sup> to 10<sup>5</sup> cells ml<sup>-1</sup> (Partensky et al. 1999). Thus, *P. marinus* is the most abundant photosynthetic organism in the world playing a crucial role in global

**Electronic supplementary material** The online version of this article (doi:10.1007/s11120-017-0418-3) contains supplementary material, which is available to authorized users.

✉ Ondřej Prášil  
prasil@alga.cz

<sup>1</sup> Institute of Microbiology, Czech Academy of Sciences, v. v. i., Novohradská 237, Třeboň 37981, Czech Republic

<sup>2</sup> Department of Experimental Plant Biology, Faculty of Science, University of South Bohemia, Branišovská 31, České Budějovice 37005, Czech Republic

<sup>3</sup> Department of Microbiology, Oregon State University, Nash Hall, Corvallis, OR 97330, USA

primary production and carbon cycling (Chisholm et al. 1988; Partensky et al. 1999).

*Prochlorococcus* contributes an estimated 13–48% of NPP in the equatorial Pacific Ocean (Vaulot et al. 1995) and an estimated 8.5% of ocean NPP (Flombaum et al. 2013). NPP is defined as the rate of photosynthetically fixed C available for other trophic levels, and it can be calculated as the product of phytoplankton growth rate and cell carbon when those values are available. However, while phytoplankton carbon is now measureable (Graff et al. 2012), methods to reliably determine growth rate remain out of reach. In contrast, cell chlorophyll (Chl) and light absorption are relatively simple to measure in the field and by remote sensing. Therefore, estimates of marine primary production are commonly derived using photosynthetic efficiencies [rates of carbon fixation or oxygen production per unit Chl or normalized to absorbed light (Silsbe et al. 2015)]. However, phytoplankton adjust their Chl content depending on nutrient availability. This cellular plasticity can cause the Chl:C ratio to vary by an order of magnitude and causes major uncertainties in global estimates of primary production (Siegel et al. 2013).

Rates of carbon production are commonly measured using  $^{13}\text{C}$  or  $^{14}\text{C}$ -radiolabeled sodium bicarbonate. Chl-specific  $^{14}\text{C}$ -uptake rates have been used extensively to estimate net carbon primary production (NPC) and are also used to calibrate algorithms of NPC based on satellite retrievals (Behrenfeld and Falkowski 1997). However, Chl-specific  $^{14}\text{C}$ -uptake rates vary depending on incubation duration and growth rate and can range between gross and net carbon production (Laws et al. 2002; Marra 2009). This variability is caused by the relative distribution of photosynthetically assimilated carbon among different metabolic pathways, such as various catabolic and biosynthesis pathways. Ultimately, the lifetime of newly assimilated carbon (the time it takes for assimilated carbon to be converted back to  $\text{CO}_2$ ) depends on the metabolic pathway that dominates under certain environmental conditions (Halsey et al. 2011).

In this study, we investigated the effects of nitrogen limitation on metabolic processes underlying gross and net carbon primary production and other cell properties in *P. marinus*. In recent studies on eukaryotic algae, Halsey et al. (2010, 2013, 2014) discovered that chlorophyll-specific gross and net carbon primary production ( $\text{GPC}^b$  and  $\text{NPC}^b$ ) were independent of nutrient-limited growth rates. We tested whether these behaviors are also expressed in the cyanobacterium *P. marinus*. We used  $^{14}\text{C}$ -uptake measurements of varying duration to assess  $\text{GPC}^b$  and  $\text{NPC}^b$ , fluorometry to examine Photosystem II activity (maximal photosynthetic efficiency of PSII  $F_v/F_M$ , and functional absorption cross section of Photosystem II  $\sigma_{\text{PSII}}$ ), and Fourier transform infrared (FTIR) spectroscopy to determine the biochemical composition of *P. marinus* grown at different steady-state nutrient-limited growth rates under constant saturating light (see Table 1 for detailed definitions of the production measurements made in this study). We found that *P. marinus* uses the same general carbon allocation strategies as many eukaryotic algae. However, a key difference is that the efficiency of carbon conversion into biomass is significantly lower in this globally important cyanobacterium compared to the eukaryotes (Halsey et al. 2013, 2014). Our results provide important cell properties of *Prochlorococcus* under steady-state nutrient limitation and information about the photo-physiology and photosynthetic energy use efficiency of *P. marinus* that can be directly applied to global estimates of net primary production that take into account community composition.

## Materials and methods

### Culture conditions

*Prochlorococcus marinus* strain PCC 9511 (Pasteur Culture Collection of Cyanobacteria; Pasteur Institute, Paris, France) was grown at 20 °C in chemostat mode in artificial sea water PCR-S11 medium (Rippka et al. 2000) made

**Table 1** Abbreviations and definitions of production measurements

Abbreviation	Definition	Units
$F_v/F_M$	Maximum photochemical efficiency of open RCIIIs	Unitless
$\Phi_{\text{PSII}}$	Effective photochemical efficiency of RCIIIs in actinic light	Unitless
$P_{\text{max}}^b$	Maximum Chl-specific carbon fixation rate	$\mu\text{mol C (mg DV-Chl } a \text{ h)}^{-1}$
$\alpha^b$	Light-limited slope of the PE curve	$\mu\text{mol C (mg DV-Chl } a \text{ h)}^{-1} \text{ h}^{-1}$ $(\mu\text{mol quanta m}^{-2} \text{ s}^{-1})^{-1}$
$E_k$	Light saturation point	$\mu\text{mol quanta m}^{-2} \text{ s}^{-1}$
$P_{\text{Eg}}^b$	Chl-specific carbon fixation rate at the growth irradiance	$\mu\text{mol C (mg DV-Chl } a \text{ h)}^{-1}$
$\text{GPC}^b$	Chl-specific gross carbon primary production	$\mu\text{mol C (mg DV-Chl } a \text{ h)}^{-1}$
$\text{NPC}^b$	Chl-specific net carbon primary production	$\mu\text{mol C (mg DV-Chl } a \text{ h)}^{-1}$

of Red Sea salt (Red Sea Fish Pharm, Israel) and supplemented with  $(\text{NH}_4)_2\text{SO}_4$  concentrations of 400, 200, and 100  $\mu\text{M}$  to achieve specific growth rates ( $\mu$ ) of 0.3, 0.2, and 0.1  $\text{day}^{-1}$ , respectively. The maximum specific growth rate (0.3  $\text{day}^{-1}$ ) corresponded to the N-replete culture. Cultures attained steady-state growth by continuous flow of medium into and out of the culture using peristaltic pumps at pre-set rates; accordingly,  $\mu$  was set by the dilution rate determined as

$$\mu = \frac{\text{Flow rate}}{\text{Culture volume}}. \quad (1)$$

Cultures were maintained at each growth condition for at least 10–15 generations (i.e., 3–14 weeks, depending on growth rate) to ensure full acclimation prior to sampling (LaRoche et al. 2010). Cells were considered to be at steady-state once measurements of intrinsic fluorescence ( $F_0$ ) or divinyl chlorophyll *a* (DV-Chl *a*) (see below) were constant for 3–4 consecutive days. For each nitrogen-limited growth rate, triplicate 700 ml cultures were grown in 1 l Erlenmeyer flasks, aerated, and continuously illuminated by fluorescent light bulbs (PILA LF 36W/33–640, Poland) with a photon flux density  $\sim 50 \mu\text{mol quanta m}^{-2} \text{s}^{-1}$  measured using a spherical quantum sensor (Walz ULM 500, Germany). Growth under continuous irradiance limited the range of growth rates achieved compared to those previously reported for *P. marinus* cells growing under light–dark cycles. We used constant light conditions to ensure that cell division was asynchronous and there was no diel rhythm in photosynthesis, thus providing us the advantage of reproducible sampling. *P. marinus* was unable to maintain growth at continuous irradiances  $> 50 \mu\text{mol quanta m}^{-2} \text{s}^{-1}$  (data not shown), which resulted in bleaching of cultures probably due to accumulated photo-damage. Nevertheless, the light conditions used in this study for *P. marinus* were similar to the study by Lindell et al. (2002) that investigated nitrogen metabolism in *Prochlorochoccus* strain PCC 9511.

### Culture monitoring

Daily measurements of  $F_0$  or DV-Chl *a* concentration were used to monitor each culture.  $F_0$  was measured in fluorometer FL3000 (Photon System Instrument, Czech Republic) after acclimating cells for 10 min to darkness. To determine DV-Chl *a*, cells of triplicate culture samples were filtered onto 25-mm glass fiber filters with a particle retention of 0.4  $\mu\text{m}$  (MN GF 5, Macherey–Nagel, Germany). Filters were extracted in 100% methanol and stored at  $-20^\circ\text{C}$  for 24 h. The absorption spectra of the extracts were measured spectrophotometrically (spectrophotometer UV 500, ChromSpec, CZ), and DV-Chl *a* was quantified using the equation for Chl *a* assessment in Porra (2006).

### Cell density

Number of cells was measured using a flow cytometer A50 (Apogee Flow systems, UK) equipped with a blue laser (488 nm) and analyzed using FlowJo software (FlowJo LLC, USA) using standard procedures for data analysis according to Shapiro (2005).

### Elemental composition

For cellular carbon and nitrogen analysis (C:N), 1, 2, and 3 ml samples were filtered in triplicate onto pre-combusted (5 h at  $550^\circ\text{C}$ ) MN GF 5 filters, wrapped in tin capsules and stored at  $-70^\circ\text{C}$  until analysis with a CN Elemental Analyzer vario MICRO cube (Elementar Analysensysteme GmbH, Germany) as described in Nelson and Sommers (1996). A filter blank was subtracted from raw values.

### Photosystem II Chl *a* fluorescence characteristics

Chl *a* fluorescence was measured using a fluorometer FL3000 (Photon System Instruments, Czech Republic). Cells were dark acclimated for 10 min prior to measurements to oxidize all PSII reaction centers.  $F_0$  was measured using low-intensity blue measuring light (455 nm). A multiple turnover saturating flash (duration 850 ms, intensity  $2100 \mu\text{mol quanta m}^{-2} \text{s}^{-1}$ , 635 nm) was applied to reduce all reaction centers and raise fluorescence to its maximum ( $F_M$ ). The maximum photochemical efficiency of open RCII was calculated as the ratio of  $F_V/F_M$ , where  $F_V$  (variable fluorescence) corresponds to  $F_M - F_0$ . Cells were then exposed to an actinic light ( $205 \mu\text{mol quanta m}^{-2} \text{s}^{-1}$ , 635 nm) for 145 s. The effective photochemical efficiency of PSII in actinic light ( $\Phi_{\text{PSII}}$ ) was determined as  $F_q'/F_M'$ , where  $F_M'$  is the maximum fluorescence in light-adapted state and  $F_q' = F_M' - F'$ , where  $F'$  is the steady-state fluorescence in the light (Kromkamp and Forster 2003).

### Measurements of electron transport rate

The electron transport rate (ETR) through Photosystem II was determined by fast repetition rate fluorescence using a custom-designed FL3500 fluorometer (Photon Systems Instruments, Czech Republic). After a 10 min dark acclimation period, a series of 100 blue (463 nm) flashlets of 1  $\mu\text{s}$  duration was applied to induce single turnover of all RCII. Changes in fluorescence were then measured during sequential exposure to 11 different intensities ( $0$ – $1023 \mu\text{mol photons m}^{-2} \text{s}^{-1}$ ) of blue actinic light. The resulting fluorescence light curves were fitted to the model of Kolber et al. (1998) to derive the maximum and minimal fluorescence, the effective PSII cross section ( $\sigma_{\text{PSII}}$ ), and the connectivity between photosystems ( $p$ ). These parameters

were then used to calculate the ETR according to Suggett et al. (2010):

$$\text{ETR} = \sigma_{\text{PSII}} \times n_{\text{PSII}} \times \frac{F'_q/F'_m}{F_v/F_m} \times \Phi_{\text{RCII}} \times E, \quad (2)$$

where  $n_{\text{PSII}}$  represents the ratio of functional reaction centers of PSII to total chlorophyll *a*. The value  $1/n_{\text{PSII}}=500$  (mol chl *a*/mol RCII) was used (see Suggett et al. 2010 for details).  $\Phi_{\text{RCII}}$  is the quantum yield of photochemistry within RCII [taking constant values of 1 mol e<sup>-</sup> (mol photons<sup>-1</sup>)], and  $E$  is the intensity of the actinic light. We used a custom-designed fluorometer, so an instrument-specific  $K_r$  coefficient for  $n_{\text{PSII}}$  assessment has not been determined. Therefore, relative numbers of active RCII, instead of absolute numbers, were derived from  $F_0$  and  $\sigma_{\text{PSII}}$  (Oxborough et al. 2012; Silsbe et al. 2015).

### Short-term <sup>14</sup>C-uptake rates

To assess photosynthesis versus irradiance (PE) relationships, uptake of <sup>14</sup>C-bicarbonate at light intensities ranging from 0.5 to 500 μmol quanta m<sup>-2</sup> s<sup>-1</sup> was measured in a temperature-controlled photosynthetron-type incubator. For each PE curve, a 45 ml culture aliquot was inoculated with 5 μCi inorganic <sup>14</sup>C (NaH<sup>14</sup>CO<sub>3</sub>, MP Biomedicals, CA, USA), aliquoted into scintillation vials (1 ml each), and incubated for 20 min. After incubation, samples were acidified with 50 μl 1 N HCl and degassed for 24 h. Three 1 ml samples inoculated with <sup>14</sup>C were kept in the dark for 20 min, acidified, and degassed. After 24 h of degassing, EcoLite scintillation cocktail (MP Biomedicals, CA, USA) was added to each sample to determine their radioactive decay using a Tri-Carb 2810 TR liquid scintillation analyzer (PerkinElmer, MA, USA). To obtain the total activity of NaH<sup>14</sup>CO<sub>3</sub> added, three 50 μl samples were added to vials containing 50-μl ethanolamine, 900 μl culture media, and 5 ml of EcoLite scintillation cocktail and capped immediately and counted. PE curves were modeled according to nonlinear least-squares regression described by (Jassby and Platt 1976)

$$P^b = P_{\text{max}}^b \left[ 1 - \exp\left(-\frac{\alpha^b \times E}{P_{\text{max}}^b}\right) \right], \quad (3)$$

where  $P^b$  is the Chl-specific rate of carbon fixation [μmol C (mg DV-Chl *a* h)<sup>-1</sup>],  $P_{\text{max}}^b$  is the maximum Chl-specific C fixation rate [μmol C (mg DV-Chl *a* h)<sup>-1</sup>],  $\alpha^b$  is the light-limited slope of the PE curve [μmol C (mg DV-Chl *a*)<sup>-1</sup> h<sup>-1</sup> (μmol quanta m<sup>-2</sup> s<sup>-1</sup>)<sup>-1</sup>], and  $E$  is the irradiance

(μmol quanta m<sup>-2</sup> s<sup>-1</sup>). The light saturation point  $E_k$  (μmol quanta m<sup>-2</sup> s<sup>-1</sup>) was defined as

$$E_k = \frac{P_{\text{max}}^b}{\alpha^b}. \quad (4)$$

Samples for measuring dissolved organic carbon (DOC) were prepared with <sup>14</sup>C as described above and incubated for 20 min at 0 and 500 μmol quanta m<sup>-2</sup> s<sup>-1</sup>. Samples were then filtered through an MN GF 5 filter to separate dissolved from particulate matter, acidified, and degassed as described above.

### Time dependence of <sup>14</sup>C-uptake

To determine the kinetics of <sup>14</sup>C-uptake over time, a 100 ml aliquot of culture was transferred to a small sterile temperature-controlled chemostat with the same light conditions and a flow rate adjusted to maintain the same specific growth rate as the stock chemostat by accounting for the reduced volume in Eq. (1). Freshly prepared bovine carbonic anhydrase (Sigma-Aldrich, St. Louis, MO, USA) was added to the culture (5 U ml<sup>-1</sup>) to ensure immediate isotopic equilibrium between HCO<sub>3</sub><sup>-</sup> and CO<sub>2</sub>. After 2 min, the culture was inoculated with NaH<sup>14</sup>CO<sub>3</sub> (1 μCi ml<sup>-1</sup>). Sampling for <sup>14</sup>C-uptake rate started 2 min after inoculation with <sup>14</sup>C and continued regularly over 24 h by taking 1.1 ml samples at each time point using a syringe and transferring the sample to a 2-ml Eppendorf tube. Two 0.5 ml subsamples were transferred to scintillation vials, acidified and degassed for 24 h. At each time point, two additional 50 μl samples were taken to determine the total remaining activity, and treated as total activity samples described above. Five milliliter of scintillation cocktail was added to each sample after 24 h and then measured by liquid scintillation counting.

### Generalized model of carbon utilization

Carbon allocation in cells growing at all three growth rates was modeled by calculating the fraction of newly fixed carbon that is partitioned into either a short-half-life or long-half-life pool as described in detail in Halsey et al. (2013).

### Gas exchange measurements

Photosynthesis and light-dependent respiration rates at 20 °C were measured using a MIMS (Membrane Inlet Mass Spectrometer). The instrument, experimental procedures, and data analysis were identical to Milligan et al. 2007 with the following exceptions: because *Prochlorococcus* photosynthetic activity is inhibited by stirring or shaking, we have added the isotope label by mixing 1 ml of <sup>18</sup>O<sub>2</sub>

saturated medium with 5 ml of cell suspension. The actinic illumination was provided by a laboratory white LED light source adjusted to  $50 \mu\text{mol quanta m}^{-2} \text{s}^{-1}$  inside the measuring chamber.

### Fourier transform infrared spectroscopy

To determine the macromolecular composition of cells growing at each nitrogen-limited growth rate, 30 ml of the cell suspension was harvested by centrifugation at  $8000 \times g$  for 10 min at  $20^\circ\text{C}$ . Cells were washed twice with ammonium formate ( $28 \text{ g l}^{-1}$ ), re-suspended in  $50 \mu\text{l}$  of ammonium formate, and spread on a Si 384-well plate (Bruker, Billerica, MA, USA). Samples were measured on a Nicolet IS10 (Thermo Scientific, Waltham, MA, USA) spectrometer equipped with a microarray reader and a deuterated triglycine sulfate (DTGS) detector. Absorbance spectra were collected in the spectral range from  $400$  to  $4000 \text{ cm}^{-1}$  at a spectral resolution of  $4 \text{ cm}^{-1}$  and 64 scans were co-added and averaged. A Blackman–Harris three-term apodization function was used, with a zero-filling factor of two. Omnic software (Nicolet) was used for measurement and data processing. Spectra were normalized to the maximum of an amide I absorption band at  $1645 \text{ cm}^{-1}$  and absorption maxima of lipids ( $1735 \text{ cm}^{-1}$ ) to protein (amide I) and lipid to carbohydrate ( $1152 \text{ cm}^{-1}$ ) were used for comparison (Giordano et al. 2001).

### Statistics

Data were statistically analyzed by linear regression using MS EXCEL 2010. One-way ANOVA analysis [Dunn's Method to detect significant differences ( $p < 0.05$ )] and nonlinear least-squares regressions were performed by SigmaPlot 11 (Systat Software, CA, USA).

## Results

### Growth and cell properties

Continuous cultures of *P. marinus* were established with three steady-state N-limited specific growth rates (0.1, 0.2, and  $0.3 \text{ day}^{-1}$ ). The maximum achieved growth rate of N-replete culture ( $0.3 \text{ day}^{-1}$ ) in our experiments was less than the maximal growth rate reported under light–dark regimes of illumination [ $0.69 \text{ day}^{-1}$  in synchronized cyclostats with diel light (Bruyant et al. 2005) and  $0.63 \text{ day}^{-1}$  under a 12:12 light:dark cycle (Kulk et al. 2012)]. The slower growth under continuous irradiance has been observed in several species (Brand and Guillard 1981). Recently, we reported slower growth in alga *Chromera velia* grown under light–dark cycles than

under continuous irradiance with the same light dose (Quigg et al. 2012). This has several possible reasons. Under continuous irradiance, cell cycles are not synchronized. While under light–dark cycles DNA replication and cell division occur in the dark phase, in continuous light replicated DNA is damaged and growth is inhibited. Also, in our study of *Prochlorococcus*, we used an artificial seawater-based medium with defined nitrogen concentrations instead of the natural seawater-based medium with undefined nitrogen concentrations used in the studies achieving faster growth rates. Nevertheless, the growth rates we established are comparable to those reported in other research on *P. marinus*, where  $\mu = 0.38 \text{ day}^{-1}$  under a 12:12 L:D regime (Fu et al. 2007) and  $\mu = 0.19\text{--}0.38 \text{ day}^{-1}$  under a dynamic irradiance (Kulk et al. 2011; Zorz et al. 2015) were observed. The range of growth rates used in our experiments allowed us to investigate the effects of steady-state nutrient limitation on cell properties and photosynthetic energy use in *P. marinus*.

Cellular DV-Chl *a* decreased with increasing nitrogen limitation ( $p < 0.05$ ). Thus, DV-Chl*a*:C and DV-Chl*a*:N also decrease significantly ( $p < 0.05$ , Table 2). On the other hand, ratios of C:N increased slightly but not significantly with increasing N limitation (Table 2).

### Photosystem II Chl *a* fluorescence characteristics

$F_v/F_M$  and  $\Phi_{\text{PSII}}$  remained almost invariant across all steady-state N-limited growth rates, suggesting that cells maintained fully functional active photosystems and photosynthetic electron transport regardless of the degree of nutrient limitation. The functional absorption cross section of PSII ( $\sigma_{\text{PSII}}$ ) was significantly larger in N-replete cells growing at  $0.3 \text{ day}^{-1}$  than in N-limited cells growing at 0.2 and  $0.1 \text{ day}^{-1}$  (Table 3), ( $p < 0.05$ ). Thus, *Prochlorococcus* cells decreased the size of their light-harvesting antennae with increasing N limitation. However, the

**Table 2** Cellular DV-Chl *a* content and elemental composition of steady-state nitrogen-limited cultures of *P. marinus* ( $n = 4$ ,  $\pm$  standard deviations)

Variables	N-limited growth rate ( $\text{day}^{-1}$ )		
	0.1	0.2	0.3
DV-Chl <i>a</i> (fg/cell)	$0.3 \pm 0.2^*$	$0.9 \pm 0.1^*$	$1.5 \pm 0.2^*$
DV-Chl <i>a</i> :C ( $\times 10^{-2}$ ) ( $\mu\text{g}/\mu\text{g}$ )	$0.7 \pm 0.1^*$	$1.8 \pm 0.5$	$3.1 \pm 0.7^*$
DV-Chl <i>a</i> :N ( $\mu\text{g}/\mu\text{g}$ )	$0.07 \pm 0.01^*$	$0.13 \pm 0.04^\dagger$	$0.22 \pm 0.05^{*\dagger}$
C:N ( $\mu\text{g}/\mu\text{g}$ )	$8.3 \pm 1.2$	$8.1 \pm 0.9$	$7.2 \pm 0.5$

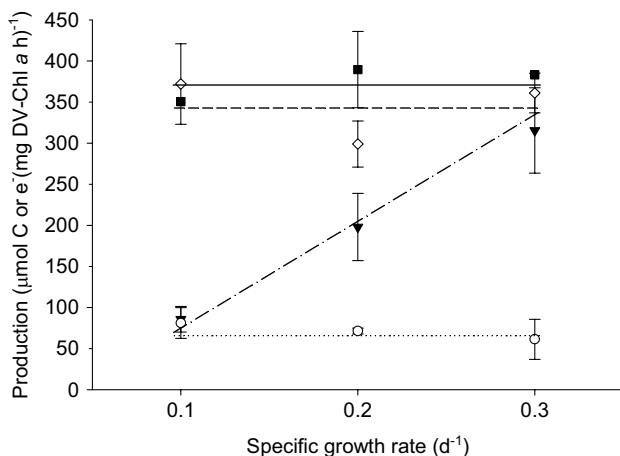
Statistically significant changes are indicated with asterisks and daggers ( $p < 0.05$ )



**Table 3** Photophysiological fluorescence characteristics of steady-state nitrogen-limited *P. marinus* ( $n=4$ ,  $\pm$ standard deviations)

Variables	N-limited growth rate ( $\text{day}^{-1}$ )		
	0.1	0.2	0.3
$F_v/F_M$	$0.63 \pm 0.03$	$0.66 \pm 0.02$	$0.62 \pm 0.01$
$\Phi_{\text{PSII}}$	$0.49 \pm 0.05$	$0.54 \pm 0.05$	$0.5 \pm 0.04$
$\sigma_{\text{PSII}}$ ( $\text{A}^2 \text{PSII}^{-1}$ )	$174 \pm 19.9^*$	$162 \pm 14.5^\dagger$	$250 \pm 5.4^{*\dagger}$
$n_{\text{PSII}}$ (PSII DV-Chl $a^{-1}$ ) relative units	$2.78 \pm 1.77$	$1.15 \pm 0.54$	$0.87 \pm 0.18$
$n_{\text{PSII}}$ (PSII cell $^{-1}$ ) relative units	$3.1 \pm 2.5$	$4.6 \pm 3.6$	$5.0 \pm 1.3$

Statistically significant changes are indicated with asterisks and daggers ( $p < 0.05$ )

**Fig. 1** Relationships between the photosynthetic electron transfer rate (open diamond and dashed line), DV-Chl *a* specific gross carbon primary production ( $\text{GPC}^b$ , filled square and solid line), carbon fixation rate at the growth irradiance ( $P_{\text{Eg}}^b$ , filled inverted triangle and dash-dotted line), and net carbon primary production ( $\text{NPC}^b$ , open circle and dotted line), in *P. marinus* as a function of N-limited growth rate. Each data point is the average from at least three measurements (where none are visible, the error bars are smaller than the size of the symbol)

decrease in effective PSII antenna size was not linearly proportional to the nutrient-dependent decline in growth rate and in chlorophyll concentration. We hypothesize that this nonlinearity in  $\sigma_{\text{PSII}}$  dependence on the growth rate and pigmentation reflects the removal of the packaging effect (i.e., pigment self-shading) in the N-limited cells growing at 0.2 and 0.1  $\text{day}^{-1}$ . Relative  $n_{\text{PSII}}$  normalized to DV-Chl *a* increased with increasing nutrient limitation, but, conversely, when normalized to cell density, relative  $n_{\text{PSII}}$  decreased (Table 3). Photosynthetic electron transfer rates through PSII at the growth irradiance did not change across steady-state N-limited growth rates and averaged  $344 \pm 39 \mu\text{mol e}^- (\text{mg DV-Chl } a \text{ h}^{-1})$  (Fig. 1).

### Short-term $^{14}\text{C}$ -uptake incubations

Chl-specific 20 min  $^{14}\text{C}$ -uptake measurements were used to estimate photosynthesis as a function of irradiance (PE

**Table 4** Variables describing PE curves measured in steady-state nitrogen-limited *P. marinus* ( $n=3$ ,  $\pm$ standard deviations)

Variables	N-limited growth rate ( $\text{day}^{-1}$ )		
	0.1	0.2	0.3
$P_{\text{max}}^b$ [ $\mu\text{mol C}$ (mg DV-Chl $a \text{ h}^{-1}$ ) $^{-1}$ ]	$214 \pm 4^*$	$316 \pm 4^*$	$558 \pm 6^*$
$\alpha^b$ [ $\mu\text{mol C}$ (mg DV-Chl $a$ ) $^{-1} \text{h}^{-1}$ ( $\mu\text{mol quanta m}^{-2} \text{s}^{-1}$ ) $^{-1}$ ]	$3 \pm 0.1^*$	$6 \pm 0.2^*$	$11 \pm 0.3^*$
$E_k$ ( $\mu\text{mol quanta m}^{-2} \text{s}^{-1}$ )	$71 \pm 0.8^*$	$53 \pm 1.5$	$51 \pm 1.8$
$P_{\text{Eg}}^b$ [ $\mu\text{mol C}$ (mg DV-Chl $a \text{ h}^{-1}$ ) $^{-1}$ ]	$86 \pm 16^*$	$198 \pm 41^*$	$315 \pm 52^*$
$P_{\text{C}}^b$ ( $\text{day}^{-1}$ )	$0.17 \pm 0.03^*$	$1.02 \pm 0.21^*$	$2.18 \pm 0.46^*$
DOC% of $P_{\text{max}}^b$	$19 \pm 3.2^*$	$7 \pm 1.1$	$6 \pm 2.5$

Statistically significant changes are indicated with asterisks ( $p < 0.05$ )

curves) and to gain information about how nutrient limitation influences carbon metabolism. From the fits of the measured data, we determined the initial light-limited slope ( $\alpha^b$ ) and the light-saturated rate of carbon fixation ( $P_{\text{max}}^b$ ). Both  $P_{\text{max}}^b$  and  $\alpha^b$  increased linearly ( $r^2=0.96$ ) with  $\mu$  (Table 4; Fig. 2). The consequence of the observed covariance in  $P_{\text{max}}^b$  and  $\alpha^b$  is that the light saturation index ( $E_k$ ) was almost identical for  $\mu=0.3$  and 0.2  $\text{day}^{-1}$  (Behrenfeld et al. 2004), and  $E_k$  was only slightly higher in the severely nitrogen-limited cells with  $\mu=0.1 \text{ day}^{-1}$  (Table 4). From the PE curves generated from 20 min incubations, we also determined  $P_{\text{Eg}}^b$ , which is the Chl-specific carbon fixation rate at the growth irradiance ( $50 \mu\text{mol quanta m}^{-2} \text{s}^{-1}$ ).  $P_{\text{Eg}}^b$  increased linearly with  $\mu$  ( $r^2=0.99$ ) and differed significantly among N-limited cultures ( $p < 0.05$ ), (Table 4; Fig. 1). At first approximation, since  $P_{\text{Eg}}^b$  was measured at the growth irradiance, it should provide quantitative information about the amount of fixed C available for cell metabolism and growth. However, due to the duration of the incubation (20 min),  $P_{\text{Eg}}^b$  represents the balance between (a) new C fixed by photosynthesis and retained by the cell and (b) new C fixed and oxidized back to  $\text{CO}_2$  during the incubation. In severely N-limited cells,  $P_{\text{Eg}}^b$  matched the  $\text{NPC}^b$  value, but  $P_{\text{Eg}}^b$  was similar to  $\text{GPC}^b$  in N-replete cells (Fig. 1). Short-term (20 min)

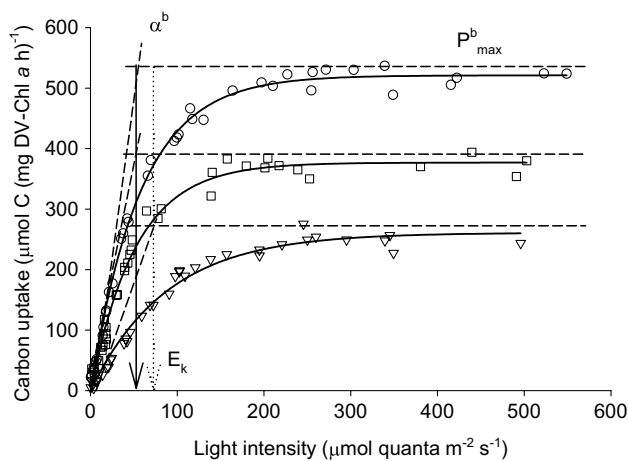


**Fig. 2** Carbon uptake rate as a function of irradiance for *P. marinus* steady-state cultures grown at 0.3 day<sup>-1</sup> (open circle), 0.2 day<sup>-1</sup> (open square), and 0.1 day<sup>-1</sup> (open inverted triangle) obtained from 20 min <sup>14</sup>C-uptake measurements. Data fitting is represented by solid lines. Parameters  $\alpha^b$  and  $P^b_{max}$  are characterized by drawn short dashed lines to show the light saturation index  $E_k$  (solid arrow for cultures grown at 0.3 day and 0.2 day<sup>-1</sup>, dashed arrow for culture grown at 0.1 day<sup>-1</sup>)

carbon fixation provided a fairly good estimate of growth rate ( $=P^b_{Eg} \times DV\text{-Chl } a/C$ ) in the slowest growing cells (0.17 day<sup>-1</sup> in cells growing at 0.1 day<sup>-1</sup>), but increasingly overestimated growth rate by five- and sevenfold in cells growing at 0.2 and 0.3 day<sup>-1</sup>, respectively (Table 4). The amount of DOC excreted into the medium was <10% of  $P^b_{max}$  in N-replete cells ( $\mu=0.3$  day<sup>-1</sup>) and in less N-limited cells ( $\mu=0.2$  day<sup>-1</sup>), but was 20% of  $P^b_{max}$  in severely N-limited cells ( $\mu=0.1$  day<sup>-1</sup>) (Table 4).

### Time-dependent <sup>14</sup>C-uptake

Because previous work showed that metabolic processing of newly fixed carbon can be influenced by nutrient limitation and therefore can impact the kinetics of carbon turnover, we also determined the time dependency of the net rate of C assimilation in *P. marinus*. Chl-specific <sup>14</sup>C-based production was measured following incubations that ranged from 2 min to 24 h using the method introduced by Halsey et al. (2011) (Fig. 3). Measurements of C-production obtained 2 min after isotope addition were similar for cultures grown at the three N-limited growth rates and averaged  $374 \pm 21$   $\mu\text{mol C (mg DV-Chl } a \text{ h)}^{-1}$ , providing a good estimate of  $GPC^b$ . Chl-specific <sup>14</sup>C-uptake rates decreased with time. The kinetics describing the decline of the Chl-specific <sup>14</sup>C-uptake rates changed depending on N limitation. In the most severely N-limited cells, Chl-specific <sup>14</sup>C-uptake declined by 50% of the initial rate after only 4 min. In contrast, it took 10 min in less N-limited cells and 120 min in N-replete cells for Chl-specific

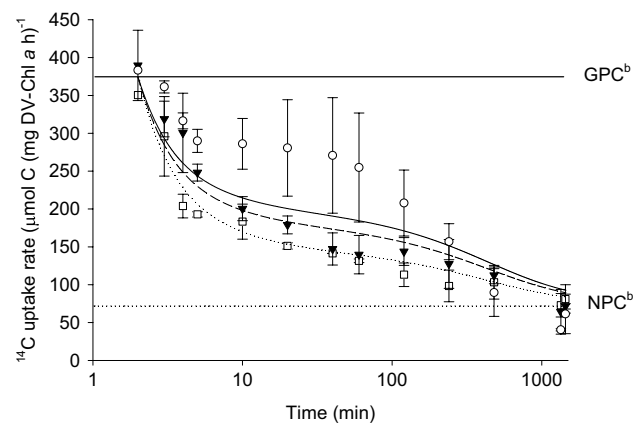


**Fig. 3** Kinetics of carbon production based on <sup>14</sup>C-uptake measurements of increasing duration and the generalized model of carbon utilization for cells growing at 0.3 day<sup>-1</sup> (open circle and solid line), 0.2 day<sup>-1</sup> (filled inverted triangle and dashed line), and 0.1 day<sup>-1</sup> (open square and dotted line). The rates of decline occurring in the <sup>14</sup>C-based production show growth rate-dependent kinetics of carbon utilization. The solid horizontal line is gross carbon primary production determined from the 2 min <sup>14</sup>C-uptake incubation, and the dotted horizontal line is net carbon primary production determined from cellular carbon and DV-chlorophyll *a* and matches the 24 h <sup>14</sup>C-uptake values for cells at all growth rates. Each data point is the average of three measurements, error bars are standard deviations with  $n=3$  (where not visible, the error bars are smaller than the size of the symbol)

<sup>14</sup>C-uptake to decline to 50% of the initial rate. Following 24 h, approximately 80% of newly fixed carbon had been catabolized to CO<sub>2</sub> regardless of growth rate. After 24 h, Chl-specific <sup>14</sup>C-uptake matched NPC<sup>b</sup> in cells growing at all growth rates. NPC<sup>b</sup> was invariant with growth rate and averaged  $71 \pm 10$   $\mu\text{mol C (mg DV-Chl } a \text{ h)}^{-1}$ .

We applied a generalized model of algal carbon allocation and mobilization (Halsey et al. 2013) to our data describing the kinetics of <sup>14</sup>C-production (Fig. 3). This model is based on the idea that newly fixed carbon is allocated to two different carbon pools that vary in their rate of carbon oxidation back to CO<sub>2</sub> in proportion to growth rate. The model gave a strong fit to the data for cells growing at the slower two growth rates ( $r^2=0.97$ ), but was a poorer fit for the fastest growing cells ( $r^2=0.86$ ). Optimized half-lives for the two carbon pools were 18 s and 2.8 h.

### Fourier transform infrared spectroscopy

We used FTIR to determine the relative contributions of different macromolecular carbon pools in *P. marinus* growing at different nutrient-limited growth rates (Pistorius et al. 2009). The biomass of faster growing cells ( $\mu=0.3$  day<sup>-1</sup>) was more biochemically reduced (i.e., containing higher amounts of proteins than slower growing cells). More severe N limitation caused carbohydrates to increase

from 32 to 43% of the total carbon content while protein content decreased from 61 to 46%, ( $p < 0.05$ ) and lipid content remained nearly constant (Fig. 4).

## Discussion

This study examined the physiological responses of *P. marinus* strain PCC 9511 to nutrient limitation. We focused on understanding how the degree of nutrient limitation affected resource allocation in this globally important cyanobacterium and whether these allocation strategies are distinct from those determined in other eubacterial and eukaryotic phototrophs.

Parameters describing the pigmentation (Table 2) show that cells decrease cellular DV-Chl *a* with increasing nitrogen limitation. Light-harvesting pigments are rich in nitrogen and are therefore downregulated with decreasing ammonium availability. This adjustment also caused the DV-Chl *a*:C and DV-Chl *a*:N ratios to decrease linearly with decreasing growth rate. Such linearity has been observed before, and the slope of the DV-Chl *a*:C vs. nutrient-limited growth rate relationship in *P. marinus* is comparable to the corresponding relationships in eukaryotic algae (Laws and Bannister 1980; Halsey and Jones 2015). This new information for numerically abundant *P. marinus* increases the robustness of the Chl:C parameter to constrain production models. Interestingly,  $F_V/F_M$  and  $\Phi_{PSII}$  in acclimated *P. marinus* cells were not affected by nitrogen limitation (Table 3) supporting the results of Parkhill et al. (2001). Thus, *P. marinus* alters its light-harvesting

photosynthetic apparatus to maintain maximal photosynthetic efficiency at the level of PSII in response to nutrient availability. Such alterations of the light-harvesting system include adjusting the effective absorption cross section ( $\sigma_{PSII}$ ). In the nitrogen-limited cells (i.e., cells growing at  $\mu = 0.1$  and  $0.2 \text{ day}^{-1}$ ), the very low cellular DV-Chl *a* content was reflected by a reduced  $\sigma_{PSII}$  and higher relative  $n_{PSII}$  compared to cells growing at  $0.3 \text{ day}^{-1}$ . However, changes in relative  $n_{PSII}$  related to DV-Chl *a* (Table 3) were driven by the decreasing concentration of DV-Chl *a* within the cell. Interestingly, the cellular density of PSII reaction centers decreased markedly with decreasing growth rate (Table 3). This result, taken together with the smaller protein pool (Fig. 4) in nitrogen-limited cells, suggested crucial changes in the PSII light-harvesting antennae (Herzig and Falkowski 1989). These changes allow cells to maintain maximal photosynthetic efficiency and photosynthetic electron transport across all growth rates (Table 3; Fig. 1).

Basic parameters describing PE relationships in N-limited *P. marinus* ( $P_{max}^b$ ,  $\alpha^b$ , and  $P_{Eg}^b$ ; see Table 4) decreased linearly with increasing N limitation.  $E_k$  thus remained constant in cells growing at  $0.3$  and  $0.2 \text{ day}^{-1}$ , a phenomenon known as  $E_k$ -independent variability. This behavior is caused by differences in how newly fixed carbon is allocated to carbon metabolic pathways depending on growth rate. In very slowly growing cells, severely limited by nitrogen, the lifetime of newly fixed carbon is much shorter compared to faster growing cells (Halsey et al. 2010, 2011). Interestingly,  $P_{max}^b$  measured in N-replete cells (Table 4) nearly matched dawn values in *P. marinus* PCC 9511 grown under cyclostat conditions (Bruyant et al. 2005). Similarly,  $P_{max}^b$  in severely N-limited cells was similar to the mid-night values in the Bruyant et al. (2005) study. Thus, the dawn- and night-time physiology of *P. marinus* growing under a diel cycle appear to express the metabolic behaviors of fast and slow-growing cells, respectively. These observations comparing photo-physiology of laboratory-based culture studies are particularly useful when interpreting measurements on natural communities to understand their nutrient or growth status.

The particular stage of the cell cycle through which a cell is progressing also influences how newly fixed carbon is allocated to different carbon metabolic pathways. During the division phase (S-G2-M), cells direct the majority of new carbon to long-term storage compounds (long-lived carbon forms) (Halsey et al. 2013). Thus,  $P_{max}^b$  peaked in the afternoon in synchronized *Prochlorococcus* MED4, coinciding with the division phase of the cell cycle (Zinser et al. 2009). Slightly less than half of the cells in our *P. marinus* culture growing at  $0.3 \text{ day}^{-1}$  divided each day, whereas only about a tenth of the cells growing at  $0.1 \text{ day}^{-1}$  divide each day. Thus, the growth rate-dependent increases in  $P_{max}^b$  and  $\alpha^b$  (Table 4) reflect the increasing proportion

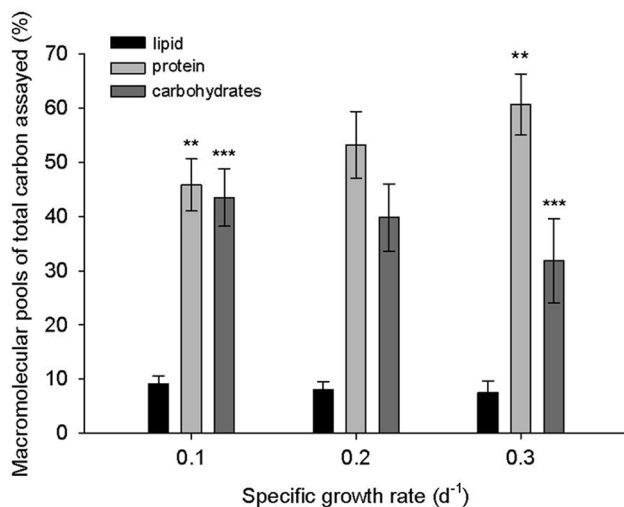


**Fig. 4** Relative macromolecular biomass composition of steady-state nitrogen-limited *P. marinus* determined by FTIR semi-quantitative analysis ( $n = 4$ ,  $\pm$  standard deviations). Changes in protein (\*\*\*) and carbohydrates (\*\*\*) content in cells grown at  $0.1$  and  $0.3 \text{ day}^{-1}$  were statistically significant from one another ( $p < 0.05$ )



of cells that are entering the division phase and diverting new carbon to longer-lived storage forms.

The rate of photosynthetic electron transport through PSII ( $ETR_{PSII}$ ) was not significantly different from  $GPC^b$  across all three N-limited growth rates (Fig. 1). This result indicates that under the growth conditions employed in this study, essentially all photosynthetically derived electrons passing through thylakoid membrane from PSII towards PSI are used for carbon fixation via the Calvin cycle. This result was surprising because previous work on *P. marinus* PCC 9511 postulated that a significant portion of photosynthetically derived electrons are diverted away from the Calvin cycle and instead directed to oxygen-consuming pathways, such as the Mehler reaction and terminal oxidase activity, to generate sufficient ATP to fuel metabolism (Behrenfeld et al. 2008). To verify our findings that these pathways were not operating in our cultures, we used  $^{18}O_2$  as a tracer of respiration and monitored its loss rates in the light and dark using MIMS. If these alternative, oxygen-consuming pathways were operating in our *P. marinus* cultures,  $^{18}O_2$  would have been consumed more rapidly in the light than in the dark (Halsey et al. 2010); however, no differences in the  $^{18}O_2$  loss rates were observed in cells grown at any of the three nitrogen-limited growth rates (Fig. S1).

One possibility for the contrasting results of these studies is that in all of our cultures, regardless of growth rate, sufficient newly fixed carbon flows through cellular catabolic pathways (glycolysis and respiration) to satisfy the ATP demands of the cells. This scenario is especially plausible because the growth rates were slow [ $0.1\text{--}0.3\text{ day}^{-1}$ , compared to  $0.69\text{ day}^{-1}$  in the Behrenfeld et al. (2008) report]. Thus, the proportion of new carbon allocated to short-lived pathways (respiration) was likely sufficient for all ATP requirements in our cultures, but it was insufficient to cover the energetic costs in cells growing faster than  $0.3\text{ day}^{-1}$ . Therefore, in fast growing cells, alternative pathways (Mehler and terminal oxidase activity) may be required but not in the slow-growing cells in our experiments. It is worth noting that phytoplankton isolated from the oligotrophic open ocean, including *P. marinus* MED4, exhibited alternative oxidase activity. This activity is highest under high-light conditions (Mackey et al. 2008). Moreover, plastoquinol terminal oxidase proteins (McDonald and Vanlerberghe 2005) and NAD(P)H dehydrogenase complexes which function in PSI cyclic electron transport were found in MED4 (Zinser et al. 2009). These findings obtained from field (McDonald and Vanlerberghe 2005; Mackey et al. 2008) and laboratory research (Behrenfeld et al. 2008; Zinser et al. 2009) suggest that *P. marinus* may activate and use alternative electron pathways in response to high light to avoid photo-damage. However, to our knowledge, oxygen-consuming alternative pathways have not yet been directly measured in *Prochlorococcus*,

and those alternative pathways were only a small fraction of gross photosynthesis in the cyanobacterium, *Microcystis aeruginosa* (Kunath et al. 2012).

It should be noted here that despite many trials, we have not yet been able to quantitatively measure the rates of oxygen evolution in *Prochlorococcus* that match the measured rates of ETR or C assimilation. For some unknown reason, the maximal gross rates of  $O_2$  evolution [ $110\text{--}145\text{ }\mu\text{mol } O_2\text{ (mg DV-chl } a\text{ h)}^{-1}$ ] measured either using a Clark electrode or MIMS were several times lower than the rates of ETR or  $GPC^b$ . Further experiments are under way to elucidate whether this is due to the mechanical stress caused by unavoidable concentrating and stirring of *Prochlorococcus* cell suspensions, or whether it is inherently caused by some structural or functional modification of Photosystem II in this organism with highly streamlined genome (e.g., Rocap et al. 2003).

The rate of carbon fixation through the Calvin cycle is GPC and the rate of carbon accumulation into biomass is NPC. Consistent with previous observations in eukaryotic algae (Halsey et al. 2010, 2013, 2014), our results showed that neither  $GPC^b$  nor  $NPC^b$  were affected by nitrogen limitation in *P. marinus*. We found that  $NPC^b$  constituted approximately 20% of  $GPC^b$ . The remaining 80% of  $GPC^b$  is known as a transient carbon pool. The primary product of the Calvin cycle is glyceraldehyde 3-phosphate and allocation of this product to different metabolic pathways is species specific (Palmucci et al. 2011; Giordano et al. 2015), and as discussed above, can also vary depending on nitrogen availability (Kaffes et al. 2010; Palmucci et al. 2011; Giordano et al. 2015; Halsey et al. 2010, 2011, 2013).

The parameter  $P_{Eg}^b$ , together with time-dependent  $^{14}C$  measurements, can reveal information about how cells alter carbon allocation in response to different environmental conditions.  $P_{Eg}^b$  matched  $NPC^b$  values in cells growing at  $\mu=0.1\text{ day}^{-1}$  (Fig. 1). Thus, in these very slowly growing cells, 80% of the carbon fixed during the 20-min incubation (the difference between  $GPC^b$  and  $NPC^b$ ) was “short-lived” transient carbon that was catabolized back to  $CO_2$ . On the other hand,  $P_{Eg}^b$  matched  $GPC^b$  in cells growing at  $\mu=0.3\text{ day}^{-1}$  because carbon fixed during the incubation is long-lived. The growth rate-dependent lifetimes of the transient carbon pool are clearly resolved in Fig. 3 and are remarkably similar to the behaviors in other nutrient-limited algae. Nevertheless, the generalized model of carbon utilization did not fully capture the kinetics of carbon production in *P. marinus* growing at  $0.3\text{ day}^{-1}$ . The data show that newly fixed carbon in cells growing at  $0.3\text{ day}^{-1}$  is longer lived than the model predicts and suggests that other processes are functioning to regulate carbon use in this bacterium.

To better understand how carbon use in *P. marinus* differs from other algae, we also compared biomass composition of *P. marinus* across nutrient-limited growth rates.

The fate of new carbon differs depending on the environment because cellular requirements for the major macromolecules, lipids, proteins, and carbohydrates, can vary with nutrient availability (Jakob et al. 2007). In general, eukaryotic cells cultivated in continuous culture respond to decreased growth rate due to increased N limitation by reducing carbon flow to lipids and accumulating carbohydrates (Halsey and Jones 2015). In *P. marinus*, we also found a significant increase in carbon allocated into carbohydrates in cells growing at 0.1 compared to 0.3 day<sup>-1</sup> (Fig. 4). However, lipid content did not change significantly and was only 8–10% of the total carbon pool compared to 45–70% in green algae (Halsey and Jones 2015; Fig. 3), likely reflecting the lack of internal membrane bound organelles in the cyanobacterium. The protein pool, which is typically maintained even at very slow growth rates (Morris 1980) became smaller with N limitation. Overall, the carbon allocation patterns in *P. marinus* grown under nitrogen limitation were equivalent to those observed in the model diatom *P. tricornutum* (Jakob et al. 2007).

One of the open questions in the field of aquatic primary productivity is whether relatively simple and rapid measurements of ETR, derived from chlorophyll variable fluorescence can substitute traditional methods employing incorporation of C isotopes in quantitative determination of primary productivity (for review, see Suggett et al. 2010). For several decades, researchers have tried to parametrize and understand the underlying mechanisms causing the observed variability between ETR and C fixation. Such variability can be quantified as the electron requirement for carbon fixation ( $\Phi_{e,C} = \text{ETR}/\text{C fixation}$ , Lawrenz et al. 2013). Our results indicate, that when C assimilation is determined by short-term incubations (20–120 min), a major source of the variability in  $\Phi_{e,C}$  seems to be environmentally driven changes in utilization of C products. Our and recent work (reviewed in Halsey and Jones 2015) show that rates of C fixation determined in such a way can attain almost any value between  $\text{GPC}^b$  (for nutrient-replete) and  $\text{NPC}^b$  (for nutrient-stressed cultures). On the other hand, in all cases reported here, ETR provided accurate estimates of  $\text{GPC}^b$  and more importantly, a vehicle for determining  $\text{NPC}^b$ . Therefore, at least for *Prochlorococcus*, aquatic net primary production can be derived directly from measurements of ETR. Further research is, however, needed to prove validity of this hypothesis for other organisms and other environmental stresses.

This work quantitatively describes the photosynthetic energy budget in the globally abundant cyanobacterium *P. marinus* strain PCC 9511. To our knowledge, this is only the second cyanobacterium for which an accounting of photosynthetic energy from gross to net photosynthesis has been done.  $\text{GPC}^b$  in *P. marinus* [ $374 \pm 21 \mu\text{mol C (DV-Chl } a \text{ h)}^{-1}$ ] was similar to the value for *D. tertiolecta*

[ $319 \pm 17 \mu\text{mol C (Chl } a \text{ h)}^{-1}$ ] (Halsey et al. 2010). However, only 20% of  $\text{GPC}^b$  was retained as  $\text{NPC}^b$  in *P. marinus*, compared to ~35% in the green alga and in a diatom (Halsey et al. 2013). Interestingly,  $\text{NPC}^b$  was only 18% of  $\text{GPC}^b$  in *M. aeruginosa*, to our knowledge the only other cyanobacterium for which these data have been collected during nitrogen-limited growth (Kunath et al. 2012). On the other hand, under light-limited growth, CO<sub>2</sub> conversion into biomass was at least as efficient in *Synechocystis* sp. as in the green alga, *Chlorella sorokiniana* (Schuurmans et al. 2015). These data suggest the possibility that under nitrogen limitation, cyanobacteria are generally less efficient in converting photosynthetic energy into biomass. This decreased energetic efficiency could be related to the fact that in cyanobacteria, photosynthetic and respiratory electron transport operate simultaneously in the plasma membrane, and moreover, these two processes share some of the same electron transfer components. Other photosynthetic electron transport pathways, such as those that contribute to light-dependent oxygen consumption (e.g., Mehler and/or midstream oxidase activities) and cyclic electron transport, can serve to supplement ATP generation, thereby decreasing reliance on carbon catabolism. Eukaryotes reliably direct ~20% of gross photosynthetic flow to light-dependent respiratory pathways during steady-state growth (Halsey and Jones 2015). However, reports so far show that cyanobacteria use these pathways only at super-saturating irradiances (Kunath et al. 2012; Schuurmans et al. 2015) or under iron limitation (Bailey et al. 2008), although electron cycling around PSII may be an important mechanism to support additional ATP generation in cyanobacteria (Ananyev et al. 2016). Finally, our results may also imply that primary and secondary endosymbiotic events leading to the evolution of eukaryotic algae afforded a greater efficiency of photosynthetic energy use.

**Acknowledgements** We wish to thank Jiří Šetlík for technical support, and Jana Hofhanzlová, Eva Žiškova, Jason Dean, and Ondřej Komárek for their assistance. This work was supported by projects MSMT Kontakt II LH11064 (to O. P.), MSMT NPU I LO 1416 (to O. P.), and GAJU 143/2013/P (to K. F.).

## References

- Ananyev G, Gates C, Dismukes GC (2016) The oxygen quantum yield in diverse algae is controlled by partitioning of flux between linear and cyclic electron flow within photosystem II. *Biochim Biophys Acta-Bioenerg* 1857:1380–1391
- Bailey S, Melis A, Mackey KRM, Cardol P, Finazzi G et al (2008) Alternative photosynthetic electron flow to oxygen in marine *Synechococcus*. *Biochim Biophys Acta-Bioenerg* 1777:269–276
- Behrenfeld JM, Falkowski PG (1997) A consumer's guide to phytoplankton primary productivity models. *Limnol Oceanogr* 42:1479–1491

- Behrenfeld JM, Prášil O, Babin M, Bruyant F (2004) In search of physiological basis for covariations in light-limited and light-saturated photosynthesis. *J Phycol* 40:4–25
- Behrenfeld JM, Halsey KH, Milligan AJ (2008) Evolved physiological responses of phytoplankton to their integrated growth environment. *Phil Trans R Soc B* 363:2687–2703
- Brand LE, Guillard RRL (1981) The effects of continuous light and light intensity on the reproduction rates of twenty-two species of marine phytoplankton. *J Exp Mar Biol Ecol* 50:119–132
- Bruyant F, Babin M, Genty B, Prášil O, Behrenfeld JM et al (2005) Diel variations in the photosynthetic parameters of *Prochlorococcus* strain PCC 9511: combined effects of light and cell cycle. *Limnol Oceanogr* 50:850–863
- Chisholm SW, Olson RJ, Zettler ER, Goericke R, Waterbury A (1988) A novel free-living prochlorophyte abundant in the oceanic euphotic zone. *Nature* 334:340–343
- Falkowski PG, Barber RT, Smetacek V (1998) Biogeochemical controls and feedbacks on ocean primary production. *Science* 281:200–206
- Field CB, Behrenfeld MJ, Randerson JT, Falkowski P (1998) Primary production of the biosphere: integrating terrestrial and oceanic components. *Science* 281:237–240
- Flombaum P, Gallegos JL, Gordillo RA, Rincón J, Zabala LL et al (2013) Present and future global distributions of the marine cyanobacteria *Prochlorococcus* and *Synechococcus*. *Proc Natl Acad Sci* 110:9824–9829
- Follows MJ, Dutkiewicz S (2011) Modeling diverse communities of marine microbes. *Annu Rev Mar Sci* 3:427–451
- Fu FX, Warner ME, Zhang Y, Feng Y, Hutchins DA (2007) Effects of increased temperature and CO<sub>2</sub> on photosynthesis, growth, and elemental ratios in marine *Synechococcus* and *Prochlorococcus* (cyanobacteria). *J Phycol* 43:485–496
- Giordano M, Kansiz M, Heraud P, Beardall J, Wood B, McNaughton D (2001) Fourier transform infrared spectroscopy as a novel tool to investigate changes in intracellular macromolecular pools in the marine microalga *Chaetoceros muellerii* (Bacillariophyceae). *J Phycol* 37:271–279
- Giordano M, Palmucci M, Norici A (2015) Taxonomy and growth conditions concur to determine the energetic suitability of algal fatty acid complements. *J Appl Phycol* 27:1401–1413
- Graff JR, Milligan AJ, Behrenfeld MJ (2012) The measurement of phytoplankton biomass using flow-cytometric sorting and elemental analysis of carbon. *Limnol Oceanogr Method* 10:910–920
- Halsey KH, Jones B (2015) Phytoplankton strategies for photosynthetic energy allocation. *Annu Rev Mar Sci* 7:265–297
- Halsey KH, Milligan AJ, Behrenfeld MJ (2010) Physiological optimization underlies growth rate-independent chlorophyll-specific gross and net primary production. *Photosynth Res* 103:125–137
- Halsey KH, Milligan AJ, Behrenfeld MJ (2011) Linking time-dependent carbon-fixation efficiencies in *Dunaliella tertiolecta* (Chlorophyceae) to underlying metabolic pathways. *J Phycol* 47:1–11
- Halsey KH, O'Malley RT, Graff JR, Milligan AJ, Behrenfeld MJ (2013) A common partitioning strategy for photosynthetic products in evolutionarily distinct phytoplankton species. *New Phytol* 198:1030–1038
- Halsey KH, Milligan AJ, Behrenfeld MJ (2014) Contrasting strategies of photosynthetic energy utilization drive lifestyle strategies in ecologically important picoeukaryotes. *Metabolites* 4:260–280
- Herzig R, Falkowski PG (1989) Nitrogen limitation in *Isochrysis galbana* (Haptophyceae). I. Photosynthetic energy conversion and growth efficiencies. *J Phycol* 25:462–471
- Hess WR, Rocap G, Ting CS, Larimer F, Stlswagen S, Lamerdin J, Chisholm SW (2001) The photosynthetic apparatus of *Prochlorococcus*: Insight through comparative genomics. *Photosynth Res* 70:53–71
- Jakob T, Wagner H, Stehfest K, Wilhelm C (2007) A complete energy balance from photons to new biomass reveals a light- and nutrient-dependent variability in the metabolic costs of carbon assimilation. *J Exp Bot* 58:2101–2112
- Jassby AD, Platt T (1976) Mathematical formulation of the relationship between photosynthesis and light for phytoplankton. *Limnol Oceanogr* 21:540–547
- Kaffes A, Thoms S, Trimborn S, Rost B, Langer G et al (2010) Carbon and nitrogen fluxes in the marine coccolithophore *Emiliana huxleyi* grown under different nitrate concentrations. *J Exp Mar Biol Ecol* 393:1–8
- Kolber ZS, Prášil O, Falkowski PG (1998) Measurements of variable chlorophyll fluorescence using fast repetition rate techniques: defining methodology and experimental protocols. *Biochim Biophys Acta-Bioenerg* 1367:88–106
- Kromkamp JC, Forster RM (2003) The use of variable fluorescence measurements in aquatic ecosystems: differences between multiple and single turnover measuring protocols and suggested terminology. *Eur J Phycol* 38:103–112
- Kulk G, Van de Poll WH, Visser RJW, Buma AGJ (2011) Distinct differences in photoacclimation potential between prokaryotic and eukaryotic oceanic phytoplankton. *J Exp Mar Biol Ecol* 398:63–72
- Kulk G, de Vries P, Van de Poll WH, Visser RJW, Buma AGJ (2012) Temperature-dependent growth and photophysiology of prokaryotic and eukaryotic oceanic picophytoplankton. *Mar Ecol Prog Ser* 466:43–55
- Kunath C, Jakob T, Wilhelm C (2012) Different phycobilin antenna organizations affect the balance between light use and growth rate in the cyanobacterium *Microcystis aeruginosa* and in the cryptophyte *Cryptomonas ovata*. *Photosynth Res* 111:173–183
- LaRoche J, Rost B, Engel A (2010) Bioassays, batch culture and chemostat experimentation. In: Riebesell U (ed) Guide to best practices for ocean acidification research and data reporting. Publication Office of the European Union, Luxembourg, pp 81–94
- Lawrenz E, Silsbe G, Capuzzo E, Ylostalo P, Forster RM et al (2013) Predicting the electron requirement for carbon fixation in seas and oceans. *PLoS ONE* 8:e58137
- Laws EA, Bannister TT (1980) Nutrient- and light-limited growth of *Thalassiosira fluviatilis* in continuous culture with implications for phytoplankton growth in the ocean. *Limnol Oceanogr* 25:457–473
- Laws EA, Sakshaug E, Babin M, Dandonneau Y, Falkowski P et al (2002) Photosynthesis and primary productivity in marine ecosystems: practical aspects and application of techniques. JGOFS Report No. 36, Bergen
- Lindell D, Erdner D, Marie D, Prášil O, Koblížek M et al (2002) Nitrogen stress response of *Prochlorococcus* strain PCC 9511 (Oxyphotobacteria) involves contrasting regulation of *ntcA* and *antI*. *J Phycol* 38: 1113–1124
- Litchman E, Klausmeier CA (2008) Trait-based community ecology of phytoplankton. *Annu Rev Ecol Evol Syst* 39:615–639
- MacKey KRM, Paytan A, Grossman AR, Bailey S (2008) A photosynthetic strategy for coping in a high-light, low nutrient environment. *Limnol Oceanogr* 53:900–913
- Marra J (2009) Net and gross primary productivity: weighing in with <sup>14</sup>C. *Aquat Microb Ecol* 56:123–131
- McDonald AE, Vanlerberghe GC (2005) Alternative oxidase and plastiquinol terminal oxidase in marine prokaryotes of the Sargasso Sea. *Gene* 349:15–24
- Milligan AJ, Berman-Frank I, Gerchman Y, Dismukes GC, Falkowski PG (2007) Light-dependent oxygen consumption in nitrogen-fixing cyanobacteria plays a key role in nitrogenase protection. *J Phycol* 43:845–852

- Morris I (1980) Paths of carbon assimilation in marine phytoplankton. In: Falkowski PG primary productivity in the sea. Springer, New York, pp 139–159
- Nelson DW, Sommers LE (1996) Total carbon, organic carbon, and organic matter. In: Sparks DL (eds) Methods of soil analysis, part 2: chemical methods. SSSA Book Series No. 5, SSSA, Madison, pp 961–1010
- Oxborough K, Moore CM, Suggett DJ, Lawson T, Chan JG, Geider RJ (2012) Direct estimation of functional PSII reaction centre concentration and PSII electron flux on a volume basis: a new approach to the analysis of Fast Repetition Rate fluorometry (FRRF) data. *Limnol Oceanogr Method* 10:142–154
- Palmucci M, Ratti S, Giordano M (2011) Ecological and evolutionary implications of carbon allocation in marine phytoplankton as a function of nitrogen availability: a Fourier transform infrared spectroscopy approach. *J Phycol* 47:313–323
- Parkhill JP, Maillet G, Cullen JJ (2001) Fluorescence-based maximal quantum yield for PSII as a diagnostic of nutrient stress. *J Phycol* 37:517–529
- Partensky F, Garczarek L (2010) *Prochlorococcus*: advantages and limits of minimalism. *Annu Rev Mar Sci* 2:305–331
- Partensky F, Hess WR, Vaulot D (1999) *Prochlorococcus*, a marine photosynthetic prokaryote of global significance. *Microbiol Mol Biol Rev* 63:106–127
- Pistorius AM, DeGrip WJ, Egorova-Zachernyuk TA (2009) Monitoring of biomass composition from microbiological sources by means of FT-IR spectroscopy. *Biotechnol Bioeng* 103:123–129
- Porra RJ (2006) Spectrometric assays for plant, algal and bacterial chlorophylls. In: Grimm B (ed) Chlorophylls and bacteriochlorophylls biochemistry, biophysics, function and applications. Springer, Berlin, pp 95–107
- Quigg A, Kotabova E, Jaresova J, Kana R, Setlik J et al (2012) Photosynthesis in *Chromera velia* represents a simple system with high efficiency. *PLoS ONE* 7:e47036
- Rippka R, Coursin T, Hess W, Lichtlé C, Scanlan DJ et al (2000) *Prochlorococcus marinus* Chisholm et al. 1992 subs. pastoris subsp. nov. strain PCC 9511, the first axenic chlorophyll  $a_2/b_2$ -containing cyanobacterium (Oxyphotobacteria). *Int J Syst Evol Microbiol* 50:1833–1847
- Rocap G, Larimer FW, Lamerdin J, Malfatti S, Chain P et al (2003) Genome divergence in two *Prochlorococcus* ecotypes reflects oceanic niche differentiation. *Nature* 424:1042–1047
- Schuermans RM, van Alphen P, Schuurmans JM, Matthijs HCP, Hellingwerf KH (2015) Comparison of the photosynthetic yield of cyanobacteria and green algae: different methods give different answers. *PLoS ONE* 10:e0139061
- Shapiro HM (2005) Data analysis. In: Practical flow cytometry. Wiley, New York, pp 225–256
- Siegel DA, Behrenfeld MJ, Maritorena S, McClain CR, Antoine D et al (2013) Regional to global assessments of phytoplankton dynamics from the SeaWiFS mission. *Remote Sens Environ* 135:77–91
- Silsbe GM, Oxborough K, Suggett DJ, Forster RM, Ihnken S et al (2015) Toward autonomous measurements of photosynthetic electron transport rates: an evaluation of active fluorescence-based measurements of photochemistry. *Limnol Oceanogr Method* 13:138–155
- Suggett DJ, Moore MC, Geider RJ (2010) Estimating aquatic productivity from active fluorescence measurement. In: Suggett DJ (ed) Chlorophyll a fluorescence in aquatic sciences: methods and applications. Springer, Dordrecht, pp 103–127
- Ting CS, Rocap G, King J, Chisholm SW (2002) Cyanobacterial photosynthesis in the ocean: the origins and significance of divergent light-harvesting strategies. *Trends Microbiol* 10:134–142
- Vaulot D, Marie D, Olson RJ, Chisholm SW (1995) Growth of *Prochlorococcus*, a photosynthetic prokaryote, in the equatorial Pacific Ocean. *Science* 268:1480–1482
- Zinser ER, Lindell D, Johnson ZI, Futschik ME, Steglich C et al (2009) Choreography of the transcriptome, photophysiology, and cell cycle of a minimal photoautotroph, *Prochlorococcus*. *PLoS ONE* 4:1–18
- Zorz JK, Allanach JR, Murphy CD, Roodvoets MS, Campbell DA, Cockshutt AM (2015) The RUBISCO to photosystem II ratio limits the maximum photosynthetic rate in picocyanobacteria. *Life* 5:403–417